*American Mineralogist, Volume 92, pages 973–976, 2007*

**LETTER**

# Crystal chemistry of hydration in aluminous orthopyroxene

**JOSEPH R. SMYTH,[1,*] KATRIN MIERDEL,[2] HANS KEPPLER,[3] FALKO LANGENHORST,[4] LEONID DUBROVINSKY,[3] AND FABRIZIO NESTOLA[5]**

[1]Department of Geological Sciences, University of Colorado, Boulder, Colorado 80309 U.S.A.
[2]Institut für Geowissenschaften, Universität Tübingen, D-72074 Tübingen, Germany
[3]Bayerisches Geoinstitut, Universität Bayreuth, D-95440 Bayreuth, Germany
[4]Institut für Geowissenschaften, Friedrich-Schiller-Universität Jena, Burgweg 11, D-07749 Jena, Germany
[5]Dipartimento di Geoscienze, Università di Padova, Corso Garibaldi 37, I-35137 Padova, Italy

## ABSTRACT

Hydrogen incorporation in aluminous orthopyroxene may control the generation of melt and dominate the seismic properties at the base of the Earth's lithosphere. To clarify the substitution mechanism of H, we have synthesized, characterized, and refined the crystal structure of this potentially significant variant of orthopyroxene. The experimentally produced crystals are small needles up to approximately $20 \times 20 \times 100$ μm in size. Electron microprobe chemical analysis indicates about 11.7 wt% $Al_2O_3$. FTIR spectra indicate 7500 ppmw $H_2O$ with absorbance features qualitatively similar to natural mantle orthopyroxenes. TEM imagery indicates that the phase is pure orthopyroxene with low concentrations of defects and inclusions. Cell-parameter refinement from single-crystal X-ray diffraction gives $a$ = 18.1876(7) Å; $b$ = 8.7352(7) Å; $c$ = 5.1789 (5) Å, $V$ = 822.79(11) Å$^3$, which is 1.2% smaller than pure Mg anhydrous orthoenstatite. The crystal structure has been refined from single-crystal X-ray intensity data measured using a rotating anode X-ray generator, micro-focused X-ray beam, and CCD detector system. The refined structure indicates about 5% vacancy in M2 and significant Al occupancy in both M1 and T2, consistent with its composition, $(Mg_{0.95,0.05})^{M2}$, $(Mg_{0.79}Al_{0.21})^{M1}$, $(Al_{0.25}Si_{0.75})^{T2}$ $Si^{T1}$ $O_6$. The existence of hydrous orthopyroxene in the mantle could absorb water released from olivine on decompression to delay the onset of melting in the spinel stability region in mantle peridotite compositions.

**Keywords:** Orthopyroxene, crystal synthesis, high-pressure studies, X-ray data, crystal structure

## INTRODUCTION

Water is perhaps the most important unconstrained compositional variable in the Earth's interior. Nominally anhydrous phases in the mantle are likely to compose a significant reservoir of water in the planet's interior (Bell and Rossman 1992; Hirschmann et al. 2005). Water incorporation into the nominally anhydrous phases of the mantle has a major effect on their physical properties such as density, seismic velocities, electrical conductivity, strength, and rheology. Water in these phases also controls the temperature of the onset of melting and so controls igneous activity and geochemical differentiation. Relative water solubility in these phases can also shift phase boundaries and thus depths of discontinuities (Wood 1995; Smyth and Frost 2002; Frost and Dolejs 2007).

The pyroxene minerals are major constituents of mafic and ultramafic rocks of the upper mantle. Orthopyroxene, *Pbca*, coexists with clinopyroxene in lherzolites, peridotites, and pyroxenites to depths of about 150 km. The common orthopyroxene is usually $En_{90}Fs_{10}$ in composition with 2 to 3 mol% wollastonite component and coexists with olivine of about $Fo_{90}Fa_{10}$ composition and a clinopyroxene of about $Di_{80}Hd_{10}En_{10}$ composition. Orthopyroxenes from mantle xenoliths containing spinel or garnet are also typically quite aluminous with 2 to 11 wt% $Al_2O_3$ (Takeda 1972; Arai and Abe 1995). Orthopyroxene typically constitutes 10 to 25 modal percent of such rocks. At temperatures and pressures higher than 7 GPa and 800 °C, the orthorhombic pyroxene transforms to a high-pressure clinoenstatite (Angel and Hugh-Jones 1994), which, like orthopyroxene, forms a phase distinct from the calcic clinopyroxene. The high-pressure clinoenstatite is space group $C2/c$ at mantle conditions but quenches to $P2_1/c$ (e.g., Smyth 1969; Arlt et al. 1998; Tribaudino et al. 2002). The calcic clinopyroxene has symmetry $C2/c$ under all conditions. Peridotites and lherzolites commonly have an accessory aluminous phase, which can be feldspar at low pressure (<1.0 GPa), spinel at intermediate pressure (1 to 2.5 GPa), and garnet at higher pressures.

Natural clinopyroxenes from high-pressure rocks can also contain a significant hydrous component, with H contents correlating with the so-called Ca-Eskola component, $CaAl_2Si_4O_{12}$.

* E-mail: joseph.smyth@colorado.edu

Water contents up to about 1800 ppm by weight $H_2O$ have been reported (Skogby et al. 1990; Smyth et al. 1991) from silica-rich eclogites containing accessory kyanite and coesite as inclusions in kimberlites. Katayama and Nakashima (2003) report up to 3020 ppm $H_2O$ in clinopyroxenes from eclogites in UHP terrains. Hydrous omphacites accommodate hydration with M2 cation vacancies (Smyth et al. 1991), but at pressures greater than about 3 GPa there is relatively little tetrahedral Al.

Natural orthopyroxenes, by contrast, contain relatively small amounts of $H_2O$, typically less than about 200 ppm by weight $H_2O$ (Bell et al. 1995), but up to 460 ppm has been reported (Skogby 2006). Al-free orthoenstatite and clinoenstatite synthesized under hydrous mantle conditions may contain somewhat larger amounts of $H_2O$. Rauch and Keppler (2002) report 867 ppm at 7.5 GPa in orthoenstatite and 714 ppm at 10 GPa in high-clinoenstatite at 1100 °C. However, Mierdel et al. (2007) report up to 8000 ppm by weight $H_2O$ in aluminous orthopyroxene synthesized at relatively low pressures (1.5 GPa), typical of hydrous mantle lithosphere conditions. They also report that the $H_2O$ content of aluminous orthopyroxene decreases with pressure to less than 1000 ppmw at 2.5 GPa, creating a minimum in water solubility in a pyrolite-composition mantle at 2.5 to 3.5 GPa. This minimum in hydrogen solubility is, therefore, coincident with the low velocity zone in most mantle models, and Mierdel et al. (2007) have suggested that the minimum in H solubility in a pyrolite mantle corresponds to the low velocity zone at the base of the mantle lithosphere. To understand the potential significance of this discovery in terms of pyroxene crystal chemistry we have undertaken a crystal structure refinement of a well-characterized, hydrous aluminous orthopyroxene.

## Experimental methods

### Synthesis

Experiments were carried out in an end-loaded piston-cylinder apparatus. Mixtures of $Mg(OH)_2$, $Al(OH)_3$, and $SiO_2$ were loaded and welded into platinum-rhodium ($Pt_{95}Rh_5$) capsules together with about 20 wt% of liquid water. The stoichiometry of the starting mixture was chosen to correspond to aluminous orthopyroxene plus small amounts of olivine and spinel or garnet. Alternating layers with low and high silica content were introduced into the capsule to reduce nucleation rates and promote the growth of larger crystals. The synthesis was carried out at 1.5 GPa and 900 °C with a run duration of 168 h. Perfectly clear and inclusion-free single crystals of orthopyroxene were picked from the charge.

### FTIR spectroscopy

Polarized infrared spectra of oriented and doubly polished crystals were measured using a Bruker IFS 125 FTIR spectrometer coupled with an IRscope I microscope (tungsten source, $CaF_2$ beam splitter, narrow-band MCT detector, Al strip polarizer on KRS 5 substrate). Figure 1 shows a typical polarized infrared spectrum. Water contents were calculated from the infrared data using the extinction coefficients of Bell et al. (1995). This calculation yielded a water content of 7500 ppm for the sample studied.

### Composition

Chemical analyses were carried out with a JEOL 8900 RL electron microprobe (15 kV, 15 nA, 120 s counting time per spot, focused beam). Analysis of this sample gave in wt% 52.63 ± 1.02 $SiO_2$, 11.69 ± 1.71 $Al_2O_3$, and 34.93 ± 1.06 MgO. The standard deviations in the analysis reflect a slight inhomogeneity of the crystal. Calculating to cations per six O atoms, we get 1.749 Si, 0.251 $Al^{IV}$, 0.208 $Al^{VI}$, 1.731 Mg, and 0.166 H, assuming full tetrahedral site occupancy. The chemical formula thus indicates that there may be slightly less octahedral than tetrahedral Al and possible cation vacancies that are charge balanced by H. However, due to possible inhomogeneity and small size of the crystal, the Al occupancies of octahedral and tetrahedral sites are the same within error based on the electron microprobe chemical analyses.

### Unit-cell parameters

A single crystal approximately 15 × 20 × 80 μm was mounted on a glass fiber. The crystal was placed on a Huber four-circle goniometer and the orientation matrix determined by means of a rotation photograph. Fifteen reflections with 2θ between 12 and 20° were each centered in eight octants using a calculated peak profile routine in the SINGLE04 software package (Ralph and Finger 1982; Angel et al. 2000). Refined cell parameters are given in Table 1. The unit-cell volume is thus about 1.2% smaller than that of pure orthoenstatite (Ghose et al. 1986).

### Crystal structure refinement

The same crystal was remounted on a Bruker SMART–APEX CCD X-ray diffractometer equipped with a rotating Mo anode X-ray generator and an Osmic focusing X-ray optic system. The orientation matrix was determined from a single-frame exposure and a full intensity data set obtained. An empirical absorption correction was performed on the data set using the routine MULABS based on the algorithm by Blessing (1995). The data set comprised a total of 5165 reflections of which 595 were less than 4σ based on counting statistics. Symmetric reflections were merged to give 972 unique reflections of which 864 were greater than 4σ. No reflections violating space group *Pbca* were observed.

Beginning with the atom parameters of Ghose et al. (1986), atom position and displacement parameters, the crystal structure was refined in space group *Pbca*, using the program SHELXL-97 (Sheldrick 1997). Scattering curves used were for $Mg^{2+}$, $Si^{4+}$ (Cromer and Mann 1968), and $O^{2-}$ (Tokonami 1965). Cation occupancy parameters were also refined and the occupancy of the M2 position refined to approximately 96%, whereas all other cation sites refined to full occupancy within one standard deviation. The refinement converged with an *R* of 4.3% for observed reflections and 4.7% for all reflections. Final position, occupancy, and displacement parameters are given in Table 2. Nearest neighbor distances and coordination polyhedron distortion and volume parameters were calculated using METRIC (Bartelmehs et al. 1993; Downs 2005) and are given in Table 3 along with corresponding parameters of pure synthetic orthoenstatite (Ghose et al. 1986).

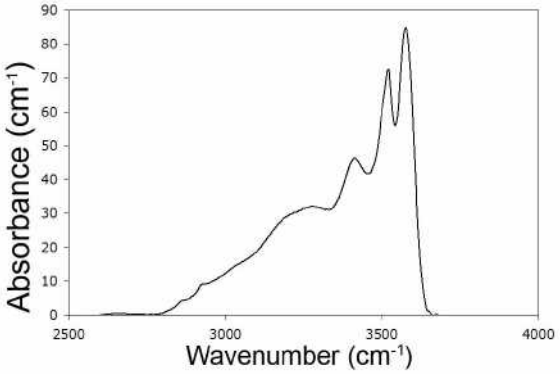


**Figure 1.** Polarized infrared absorption spectrum (E parallel *c*) of the aluminous enstatite crystal investigated in this study. Well-defined absorption features are evident at 3575, 3520, and 3411 $cm^{-1}$ with a broad feature extending to about 2800 $cm^{-1}$. The total water content of this crystal is 7500 ppm. Complete sets of polarized spectra are given in Mierdel et al. (2007).

**Table 1.** Structure refinement parameters

| Unit cell | |
|---|---|
| *a* | 18.1876(7) Å |
| *b* | 8.7352(7) Å |
| *c* | 5.1789(5) Å |
| *V* | 822.79(11) $Å^3$ |
| Space group | *Pbca* |
| $N_{meas}$ | 5165 |
| $N_{unique}$ | 972 |
| $R_{int}$ | 0.078 |
| $R_{obs}$ | 0.043 |

**Table 2.** Fractional atomic coordinates, occupancy, and displacement parameters for hydrous orthoenstatite

| Atom | *x* | *y* | *z* | occ. | $U_{11}$ | $U_{22}$ | $U_{33}$ | $U_{12}$ | $U_{13}$ | $U_{23}$ | $U_{eq}$ | Pot(V) |
|---|---|---|---|---|---|---|---|---|---|---|---|---|
| Mg1 | 0.37604(5) | 0.65378(10) | 0.86086(17) | 1.000(5) | 0.0062(6) | 0.0080(5) | 0.0042(5) | –0.0001(3) | –0.0009(3) | –0.0002(3) | 0.0061(3) | –28.5 |
| Mg2 | 0.37904(5) | 0.48367(11) | 0.35223(17) | 0.958(6) | 0.0104(6) | 0.0101(6) | 0.0054(5) | –0.0012(4) | –0.0020(4) | 0.0000(4) | 0.0086(3) | –22.8 |
| Si1 | 0.27135(4) | 0.34230(9) | 0.04527(14) | 1.000(6) | 0.0056(5) | 0.0080(5) | 0.0039(4) | –0.0006(3) | –0.0001(3) | 0.0002(3) | 0.0058(3) | –46.9 |
| Si2 | 0.47307(4) | 0.33717(8) | 0.80610(15) | 1.000(6) | 0.0068(4) | 0.0097(5) | 0.0060(5) | 0.0001(3) | 0.0002(3) | 0.0004(3) | 0.0075(3) | –45.1 |
| O1a | 0.18267(10) | 0.3391(2) | 0.0325(3) | 1.0 | 0.0057(10) | 0.0117(11) | 0.0072(9) | –0.0012(7) | –0.0010(7) | 0.0016(7) | 0.0082(5) | 27.3 |
| O2a | 0.31066(10) | 0.5049(2) | 0.0380(3) | 1.0 | 0.0084(10) | 0.0102(10) | 0.0061(9) | –0.0020(8) | –0.0005(7) | 0.0002(8) | 0.0082(5) | 27.2 |
| O3a | 0.30260(10) | 0.2233(2) | –0.1737(3) | 1.0 | 0.0079(10) | 0.0121(10) | 0.0051(8) | –0.0003(8) | 0.0001(7) | –0.0017(8) | 0.0083(5) | 31.6 |
| O1b | 0.56356(11) | 0.3374(2) | 0.8088(4) | 1.0 | 0.0077(10) | 0.0114(10) | 0.0079(10) | –0.0008(7) | 0.0016(8) | 0.0020(7) | 0.0090(5) | 25.8 |
| O2b | 0.43269(11) | 0.4854(2) | 0.6889(4) | 1.0 | 0.0091(10) | 0.0132(10) | 0.0055(9) | –0.0017(8) | –0.0011(7) | 0.0004(8) | 0.0093(5) | 25.6 |
| O3b | 0.44653(11) | 0.1910(2) | 0.6142(4) | 1.0 | 0.0079(10) | 0.0108(10) | 0.0092(10) | 0.0002(8) | 0.0010(8) | –0.0023(8) | 0.0093(5) | 29.2 |

*Notes:* *U* values in units of Å$^2$. Pot(V) = volts.

**Table 3.** Nearest neighbor distances and coordination parameters for hydrous aluminous and anhydrous pure Mg orthoenstatite

| Atoms | Hydrous | | Anhydrous |
|---|---|---|---|
| M1-O1a | 2.0090(20) | << | 2.0279 |
| M1-O1a | 2.1333(20) | << | 2.1516 |
| M1-O2a | 1.9867(20) | << | 2.0069 |
| M1-O1b | 2.1334(19) | << | 2.1709 |
| M1-O1b | 2.0346(20) | << | 2.0657 |
| M1-O2b | 2.0045(19) | << | 2.0470 |
| <M1-O> | 2.0050(20) | << | 2.0783 |
| Polyhedral Volume | 11.352 | << | 11.831 |
| Oct. Angle Variance | 27.25 | > | 26.16 |
| Quadratic Elongation | 1.0090 | = | 1.0087 |
| | | | |
| M2-O1a | 2.1279(20) | >> | 2.0891 |
| M2-O2a | 2.0566(19) | >> | 2.0335 |
| M2-O3a | 2.2846(20) | < | 2.2881 |
| M2-O1b | 2.0563(19) | ≈ | 2.0568 |
| M2-O2b | 1.9981(20) | > | 1.9920 |
| M2-O3b | 2.3139(20) | << | 2.4474 |
| <M2-O> | 2.1396(20) | < | 2.1511 |
| Polyhedral Volume | 12.254 | < | 12.464 |
| Oct. Angle Variance | 144.1 | > | 139.4 |
| Quadratic Elongation | 1.0466 | < | 1.0487 |
| | | | |
| Si1-O1a | 1.6145(19) | > | 1.6106 |
| Si1-O2a | 1.5906(19) | > | 1.5894 |
| Si1-O3a | 1.6400(18) | < | 1.6464 |
| Si1-O3a | 1.6642(18) | ≈ | 1.6672 |
| <Si1-O> | 1.6273(19) | ≈ | 1.6284 |
| Polyhedral Volume | 2.1815 | ≈ | 2.1847 |
| Tet. Angle Variance | 38.4(5) | ≈ | 39.8 |
| Quadratic Elongation | 1.0095(2) | ≈ | 1.0099 |
| | | | |
| Si2-O1b | 1.6459(20) | >> | 1.6184 |
| Si2-O2b | 1.6076(19) | >> | 1.5878 |
| Si2-O3b | 1.6885(19) | >> | 1.6775 |
| Si2-O3b | 1.6851(19) | >> | 1.6752 |
| <Si2-O> | 1.6568(19) | >> | 1.6397 |
| Polyhedral Volume | 2.3162(20) | >> | 2.2466 |
| Tet. Angle Variance | 20.9(4) | > | 19.7 |
| Quadratic Elongation | 1.0055(1) | ≈ | 1.0053 |

*Notes:* Units of bond length are angstroms, angle variance are (degrees)$^2$, and polyhedral volume are Å$^3$.

## Results and discussion

### Structure

The orthopyroxene structure consists of alternating layers of T1 (SiA) and T2 (SiB) tetrahedral chains interspersed by layers of octahedral sites containing both M1 and M2 sites in each layer. Each tetrahedral layer contains just one type of chain. Adjacent tetrahedra in each chain are related by the *c*-glide normal to *b*. Within the tetrahedral layers, adjacent T1 chains are related by a *b*-glide normal to *a*, and adjacent T2 chains are related by a $2_1$ parallel to *b*. Takeda (1972, 1973) reported that tetrahedral Al in orthopyroxene is strongly ordered in the T2 site. Domeneghetti et al. (1995) report structure systematics of orthopyroxene as a function of composition based on about 200 crystal-structure refinements of various natural samples. Although their data set is not heavily weighted with minor-element free synthetics and they have no data for H-bearing samples, their relationships do provide insight into the current sample.

### Unit-cell parameters

The *a*- and *b*-axial lengths are quite sensitive to tetrahedral Al, whereas the *c*-axis is not. The EMPA indicates 0.250 $Al^{IV}$ per formula unit in good agreement with $Al^{IV}$ calculated from the *a*-axis length using Equation 8 of Domeneghetti et al. (1995), which is 0.240. $Al^{IV}$ calculated from the *b*-axial length (Eq. 9) is 0.166. Our measured *c*-axis length is slightly shorter than any in the database of Domeneghetti et al. (1995). $Al^{IV}$ calculated from the cell volume (Eq. 14) is 0.197. So, our *a*-axial length is consistent with 0.25 Al in T2, but the *b*-axis is larger, and *c* shorter than would be predicted from tetrahedral Al content alone. This is likely due to the presence of octahedral site vacancy and protonation which are not explicitly accounted for in the structure database.

### Tetrahedral sites

Crystal-structure refinement indicates full occupancy of both tetrahedral sites with 0.6% error (Table 2). Tetrahedral Al is strongly ordered into the SiB or T2 site. It is clear from Table 2 that the SiB-O distances are all larger than for pure $Mg_2Si_2O_6$ orthopyroxene, whereas the SiA nearest neighbor distances are virtually the same. Calculating the $Al^{IV}$ in SiB from Equation 18 of Domeneghetti et al. (1995) for the mean SiB-O distance gives 0.205. The small discrepancy is likely due to the effects of octahedral cation vacancy and protonation and error in the chemical analyses.

### Octahedral sites

Crystal structure refinement indicates full occupancy of M1, but less than full occupancy of M2. Chemical analysis indicates 0.208 Al and 0.792 Mg in M1, in good agreement with Al occupancy calculated from the mean M1-O distance of 0.211 (Eq. 19, Domeneghetti et al. 1995). Crystal structure refinement indicates about 4.4% vacancy in M2, compared with about 6.2% indicated from the chemical analysis. Curiously, the M2 polyhedral volume is about 1.7% smaller than that of pure $Mg_2Si_2O_6$ orthopyroxene (Table 3). This is likely due to protonation of the O atoms in the vacant polyhedra. Final site assignments then give a structural formula of $(Mg_{0.792},Al_{0.208})^{M1}(Mg_{0.956})^{M2}H_{0.166}(Si_{1.000})^{T1}(Si_{0.749}Al_{0.251})^{T2}O_6$.

### Proton location

Polarized infrared spectra from a sample synthesized at 1100 °C and 1.5 GPa (Fig. 1) indicate that OH stretching modes in the *b*-*c* plane dominate and account for 85 to 90% of the total H. Site electrostatic potentials were calculated according to the method of Smyth (1989) using point valence charges of 2.2 for M1, 1.8 for M2, 4 for SiA, 3.75 for SiB, and –2 for each of the oxygen atoms (Table 1). Oxygen atoms O2B and O1B having the shallowest site potentials are the most likely sites of protonation. Sharp features in the infrared spectra at 3570 and 3520 $cm^{-1}$ correspond to a proton on an O-O edge of about 3.0 Å (Libowitzky 1999). The O1B-O2B edge of the M2 polyhedron is 3.01 Å and lies in the *b*-*c* plane. So as suggested previously (Stalder and Skogby 2002; Rauch and Keppler 2002; Bromiley and Bromiley 2006), this O1B-O2B edge is the most likely position for the proton, but clearly the broad absorption feature indicates much positional disorder for the proton. Also, there are more than twice as many H atoms as M2 vacancies and slightly more tetrahedral than octahedral Al, so protonation of occupied M2 polyhedral edges must also occur.

### Water in orthopyroxene

The X-ray structure refinement has shown that the main hydration mechanism in orthopyroxene is protonation of the O1B-O2B edge of vacant and occupied M2 polyhedra. This protonation requires substantial $Al^{IV}$ in the structure, but this tetrahedral Al is inhibited by increasing pressure. A decrease in tetrahedral Al with increasing pressure above 1.5 GPa is consistent with the declining H solubility in orthopyroxene at pressures of 2–3.5 GPa. Mierdel et al. (2007) suggest that decreasing H solubility in orthopyroxene with depth may result in generation of a small amount of partial melt that could account for the decrease in seismic velocities at the top of the asthenosphere. Conversely, the increase in H solubility in aluminous orthopyroxene at shallow depths may be responsible for increased rigidity of the lithospheric plates relative to the asthenosphere.

## Acknowledgments

The first author thanks U.S. National Science Foundation for grant NSF-EAR03-36611, the Bayerisches Geoinstitut Visitors Program, and the Alexander von Humboldt Foundation. This work was also supported by German Science Foundation (DFG, Leibniz award to H.K.).

## References cited

Angel, R.J. and Hugh-Jones, D.A. (1994) Equations of state and thermodynamic properties of enstatite pyroxenes. Journal of Geophysical Research, 99, 19777–19783.

Angel, R.J., Downs, R.T., and Finger, L.W. (2000) High-Temperature-High-Pressure Diffractometry. In R.M. Hazen and R.T. Downs, Eds., High-Temperature and High-Pressure Crystal Chemistry, 41, p. 559–596. Reviews in Mineralogy and Geochemistry, Mineralogical Society of America, Chantilly, Virginia.

Arai, S. and Abe, N. (1995) Reaction of orthopyroxene in peridotite xenoliths with alkali basalt melts and its implication for genesis of alpine-type chromitite. American Mineralogist, 80, 1041–1047.

Arlt, T., Angel, R.J., Miletich, R., Armbruster, T., and Peters, T. (1998) High pressure $P2_1/c$-$C2/c$ phase transitions in clinopyroxenes: Influence of cation size and electronic structure. American Mineralogist, 83, 1176–1181.

Bartelmehs, K.L., Boisen, M.B.Jr., Gibbs, G.V., and Downs, R.T. (1993) Interactive computer software used in teaching and research in mineralogy at Virginia Tech. Geological Society of America Fall Meeting, Boston, A-347.

Bell, D.R. and Rossman, G.R. (1992) Water in the Earth's mantle: The role of nominally anhydrous minerals. Science, 255, 1391–1397.

Bell, D.R., Ihinger, P.D., and Rossman, G.R. (1995) Quantitative analysis of trace OH in garnet and pyroxenes. American Mineralogist, 80, 465–474.

Blessing, R. (1995) An empirical correction for absorption anisotropy. Acta Crystallographica, A51, 33–38.

Bromiley, G.D. and Bromiley, F.A. (2006) High-pressure phase transitions and hydrogen incorporation into $MgSiO_3$ enstatite. American Mineralogist, 91, 1094–1101.

Cromer, D.T. and Mann, J. (1968) X-ray scattering factors computed from numerical Hartree-Fock wave functions. Acta Crystallographica, A24, 321–325.

Domeneghetti, M.C., Molin, G.M., and Tazzoli, V. (1995) A crystal chemical model for *Pbca* orthopyroxene. American Mineralogist, 80, 253–267.

Downs, R.T. (2005) XtalDraw for Windows. Commission on Powder Diffraction, International Union of Crystallography Newsletter, 30, 32–33.

Frost, D.J. and Dolejs, D. (2007) Experimental determination of the effect of $H_2O$ on the 410-km seismic discontinuity. Earth and Planetary Science Letters, DOI: 10.1016/j.epsl.2007.01.023.

Ghose, S., Shoemaker, V., and McMillan, R.K. (1986) Enstatite, $Mg_2Si_2O_6$, a neutron diffrsaction refinement of the crystal structure and a rigid-body analysis of the thermal motion. Zeitschrift für Kristallographie, 176, 159–175.

Hirschmann, M.M., Aubaud, C., and Withers, A.C. (2005) Storage capacity of $H_2O$ in nominally anhydrous minerals in the upper mantle. Earth and Planetary Science Letters, 236, 167–181.

Katayama, I. and Nakashima, S. (2003) Hydroxyl in clinopyroxene from the deep subducted crust: Evidence for $H_2O$ transport into the mantle. American Mineralogist, 88, 229–234.

Libowitzky, E. (1999) Correlation of O-H stretching frequencies and O-H···O hydrogen bond lengths in minerals. Monatshefte für Chemie, 130, 1047–1059.

Mierdel, K., Keppler, H., Smyth, J.R., and Langenhorst, F. (2007) Water solubility in aluminous orthpyroxene and the origin of the Earth's asthenosphere. Science, 315, 364–368.

Ralph, R.L. and Finger, L.W. (1982) A computer program for refinement of crystal orientation matrix and lattice constants from diffractometer data with lattice symmetry constraints. Journal of Applied Crystallography, 15, 537–539.

Rauch, M. and Keppler, H. (2002) Water solubility in orthopyroxene. Contributions to Mineralogy and Petrology, 142, 525–536.

Sheldrick, G.M. (1997) Shelxl-97, Program for crystal structure refinement. Göttingen University, Germany.

Skogby, H. (2006) Water in natural mantle minerals I. Pyroxenes. In H. Keppler and J.R. Smyth, Eds., Water in Nominally Anhydrous Minerals, 62, p. 155–167. Reviews in Mineralogy and Geochemistry, Mineralogical Society of America, Chantilly, Virginia.

Skogby, H., Bell, D.R., and Rossman, G.R. (1990) Hydroxide in pyroxene: Variation in the natural environment. American Mineralogist, 75, 764–774.

Smyth, J.R. (1969) Orthopyroxene—high-low clinopyroxene inversions. Earth and Planetary Science Letters, 5, 406–407.

——— (1989) Electrostatic characterization of oxygen sites in minerals. Geochimica et Cosmochimica Acta, 53, 1101–1110.

Smyth, J.R. and Frost, D. (2002) The effect of water on the 410-km discontinuity: An experimental study. Geophysical Research Letters, 29, 101485, DOI: 10.1029/2001GL014418.

Smyth, J.R., Rossman, G.R., and Bell D.R. (1991) Incorporation of hydroxyl in upper mantle clinopyroxenes. Nature, 351, 732–735.

Stalder, R. and Skogby, H. (2002) Hydrogen incorporation in enstatite. European Journal of Mineralogy, 14, 1139–1144.

Takeda, H. (1972) Crystallographic studies of coexisting aluminan orthopyroxene and augite of high pressure origin. Journal of Geophysical Research, 77, 5798–5811.

——— (1973) Tetrahedral sizes of orthopyroxenes and silicon-aluminum ordering. American Mineralogist, 58, 1096–1097.

Tokonami, M. (1965) Atomic scattering factor for $O^{2-}$. Acta Crystallographica, 19, 486.

Tribaudino, M., Nestola, F., Camara, F., and Domeneghetti, M.C. (2002) The high-temperature $P2_1/c$-$C2/c$ phase transition in Fe-free pyroxene ($Ca_{0.15}Mg_{1.85}Si_2O_6$): structural and thermodynamic behavior. American Mineralogist, 87, 648–657.

Wood, B.J. (1995) The effect of $H_2O$ on the 410-kilometer seismic discontinuity. Science, 268, 74–76.

Manuscript received January 10, 2007
Manuscript accepted February 2, 2007
Manuscript handled by Bryan Chakoumakos